CHEMISTRY OF MATERIALS
Cite This: Chem. Mater. 2018, 30, 3836−3846
Article
pubs.acs.org/cm

Anisotropic 2D $Cu_{2-x}Se$ Nanocrystals from Dodecaneselenol and Their Conversion to CdSe and $CuInSe_2$ Nanoparticles

Anne C. Berends,[†] Ward van der Stam,[†] Quinten A. Akkerman,[†] Johannes D. Meeldijk,[‡] Joost van der Lit,[†] and Celso de Mello Donega*[,†]

[†]Condensed Matter and Interfaces, Debye Institute for Nanomaterials Science, Utrecht University, P.O. Box 80000, 3508 TA Utrecht, The Netherlands

[‡]Electron Microscopy Utrecht, Debye Institute for Nanomaterials Science, Utrecht University, 3584 CH Utrecht, Netherlands

Supporting Information

ABSTRACT: We present the synthesis of colloidal anisotropic $Cu_{2-x}Se$ nanocrystals (NCs) with excellent size and shape control, using the unexplored phosphine-free selenium precursor 1-dodecaneselenol (DDSe). This precursor forms lamellar complexes with Cu(I) that enable tailoring the NC morphology from 0D polyhedral to highly anisotropic 2D shapes. The $Cu_{2-x}Se$ NCs are subsequently used as templates in postsynthetic cation exchange reactions, through which they are successfully converted to CdSe and $CuInSe_2$ quantum dots, nanoplatelets, and ultrathin nanosheets. The shape of the template hexagonal nanoplatelets is preserved during the cation exchange reaction, despite a substantial reorganization of the anionic sublattice, which leads to conversion of the tetragonal umangite crystal structure of the parent $Cu_{2-x}Se$ NCs into hexagonal wurtzite CdSe and $CuInSe_2$, accompanied by a change of both the thickness and the lateral dimensions of the nanoplatelets. The crystallographic transformation and reconstruction of the product NCs are attributed to a combination of the unit cell dimensionalities of the parent and product crystal phases and an internal ripening process. This work provides novel tools for the rational design of shape-controlled colloidal anisotropic $Cu_{2-x}Se$ NCs, which, besides their promising optoelectronic properties, also constitute a new family of cation exchange templates for the synthesis of shape-controlled NCs of wurtzite CdSe, $CuInSe_2$, and other metal selenides that cannot be attained through direct synthesis approaches. Moreover, the insights provided here are likely applicable also to the direct synthesis of shape-controlled NCs of other metal selenides, since DDSe may be able to form lamellar complexes with several other metals.

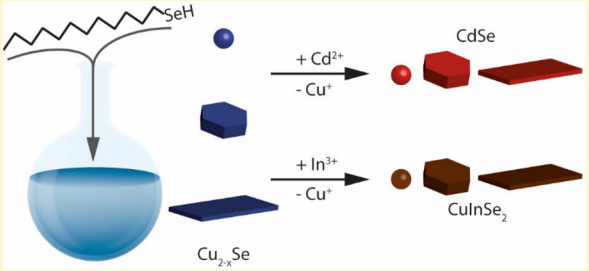

INTRODUCTION

Colloidal copper chalcogenide nanocrystals (NCs) are an emerging class of semiconductor materials with interesting optoelectronic properties, without containing heavy metals such as cadmium and lead.[1,2] Binary copper sulfide NCs can be directly synthesized in a wide range of sizes, shapes, crystal structures, and stoichiometries, which not only provides good control over their optoelectronic properties but also makes them excellent template materials for postsynthetic cation exchange reactions in order to obtain other binary or multinary metal chalcogenide NCs.[1−3] Their suitability as templates is further enhanced by the small size and charge of the Cu(I) ions and the high concentration of Cu vacancies, which facilitates fast diffusion through the lattice and easy exchange by other cations.[1−3] Nanoscale cation exchange (CE) reactions have proven to be versatile and successful synthetic routes to (hetero-)NCs with sizes, shapes, crystal structures, and compositions not (yet) realizable via direct synthesis.[4−7] Luminescent $CuInSe_2/CuInS_2$ dot core/rod shell nanorods,[8] ZnSe/ZnS dot core/rod shell nanorods,[9] ZnSe/CdSe core/shell QDs,[10] and stable and efficient (GaInZn)P QDs[11] are just a few recent examples. The key in the success of these reactions is the preservation of the anionic framework of the template NC during the CE reaction. As a result, the original size, shape, and anionic sublattice structure of the template NCs are transferred to the product NCs.[4−7] For example, it has been shown that the preservation of the anionic sublattice during Cu^+ for In^{3+} CE reactions in binary $Cu_{2-x}S$ NCs is essential to make the reaction self-limited, resulting in partial exchange to the ternary $CuInS_2$, rather than full exchange to the binary In_2S_3.[3]

However, in order to exploit the benefits of cation exchange reactions, an excellent control over size and shape is needed in the *direct* synthesis of the template NCs. Anisotropic shapes such as 1D nanorods and nanowires and 2D nanoplatelets and nanosheets of various metal chalcogenide compositions (e.g., CdA, PbA, $Cu_{2-x}A$, and ZnA, with A = S, Se, and Te) are attracting increasing attention due to their novel optoelectronic properties that hold great promise for application in spintronic devices, field-effect transistors, photodetectors, and LEDs.[12]

Received: March 17, 2018
Revised: May 9, 2018
Published: May 9, 2018

DOI: 10.1021/acs.chemmater.8b01143
Chem. Mater. 2018, 30, 3836−3846

The control of the size and shape of colloidal NCs in direct synthesis protocols requires a very strict balance of multiple physical−chemical parameters, such as temperature, reaction time, coordinating ligands, and nature and concentration of the precursors.[13] Phosphine chalcogenides (e.g., trioctylphosphine-X, TOP-X, with X = S, Se, and Te)[14−18] have been successfully used in many synthesis protocols for colloidal metal chalcogenide NCs, but their widespread use is limited by economic, safety, and environmental concerns, since phosphines are expensive, pyrophoric, and toxic chemicals. This issue can potentially be circumvented by dissolving the chalcogen directly in a noncoordinating solvent, such as octadecene (ODE),[19−21] which is however rather difficult for selenium and tellurium, due to their low solubility in noncoordinating solvents.[20,21] For metal sulfide NCs, other anion precursors have emerged as cheap and less-toxic alternatives: thiourea[1,22] and 1-dodecanethiol (DDT).[1] The latter has proven to be a versatile precursor for the synthesis of shape-controlled colloidal $Cu_{2-x}S$ NCs yielding, under suitable conditions, NCs with a wide variety of different shapes (viz., hexagonal bifrustums and bipyramids, hexagonal nanoplatelets, and ultrathin $Cu_{2-x}S$ nanosheets).[1,2,23,24] In contrast, synthesis protocols for shape-controlled colloidal $Cu_{2-x}Se$ NCs are still underdeveloped and rely almost exclusively on phosphine-based Se precursors or Se in ODE.[1,2] Recently, a selenium analogue of DDT, 1-dodecaneselenol (DDSe), was shown to be a suitable Se precursor in the solventless synthesis of Cu_2Se, Ag_2Se, and AgCuSe NCs.[25]

In this work, we show that DDSe is a very versatile Se precursor and ligand for the synthesis of colloidal $Cu_{2-x}Se$ NCs, providing excellent control over the size and shape of the NCs. By tuning the reaction parameters (viz., temperature, ligands, and halide additives), we are able to tailor the morphology of the colloidal $Cu_{2-x}Se$ NCs from 0D quantum dots to 2D nanoplatelets with varying aspect ratios and ultrathin nanosheets. $Cu_{2-x}Se$ NCs with different morphologies were subsequently used as templates in postsynthetic CE reactions to obtain CdSe and $CuInSe_2$ NCs. Interestingly, the crystal structure changes during the CE reactions from tetragonal umangite to hexagonal wurtzite. This structural transformation preserves the hexagonal shape of the nanoplatelets but changes their aspect ratio (thickness decreases, while the lateral dimensions increase). The anionic sublattice reorganization that underlies the crystallographic transformation and reconstruction of the product NCs is attributed to a combination of the unit cell dimensionalities of the parent and product phases and an internal reconstruction process, through which atoms move to the nonpolar side facets, thereby increasing the relative area of the (likely DDSe capped) polar (002) top and bottom facets. This work provides novel tools for the rational design of shape-controlled colloidal $Cu_{2-x}Se$ NCs, which, besides their promising optoelectronic properties,[1,2] also constitute a new family of cation exchange templates for the synthesis of shape-controlled NCs of wurtzite CdSe, $CuInSe_2$, and other metal selenides that cannot be attained through direct synthesis approaches. Moreover, the insights provided here are likely applicable also to the direct synthesis of shape-controlled NCs of other metal selenides, since selenolate complexes of several metals are known (e.g., Ag(I), Sn(II), Pb(II), and In(III)).[25,26]

EXPERIMENTAL SECTION

Materials. Dodecylmagnesium bromide solution (DMB, 1 M in ether), copper(I) bromide (CuBr, 98%), copper(I) acetate (CuOAc, 97%), tin(IV) tetrabromide ($SnBr_4$, 99%), tin(IV) tetrachloride pentahydrate ($SnCl_4{\cdot}5H_2O$, 98%), cadmium(II) chloride ($CdCl_2$, trace metal, 99.99%), indium chloride ($InCl_3$, trace metal, 99.99%), sodium bromide (NaBr, ≥99%), calcium chloride ($CaCl_2$, 93.0%), trioctylphosphine (TOP, 90%), 1-dodecanethiol (DDT, ≥98%), 1-octadecene (ODE, tech., 90%), trioctylphosphine oxide (TOPO, 99%), oleic acid (OA, 90%), anhydrous toluene, methanol, and butanol were purchased from Sigma-Aldrich. ODE, TOPO, and OA were degassed prior to use (120 °C under vacuum). All other chemicals were used without any further purification. Selenium powder (Se, 99.99%) was bought from Alfa Aesar.

Synthesis of 1-Dodecaneselenol (DDSe). The synthesis procedure is adapted from Froster et al.[27] Briefly, 4.56 g (57.8 mmol) of dry selenium powder was added over a period of 30 min to 60 mL of DMB solution (60 mmol) under an inert atmosphere (N_2) and refluxed for 3 h. The reaction mixture was poured over 60 mL of iced water, after which 9 mL of 37% HCl solution was added. The resulting suspension was filtered, and the organic phase of the filtrate was collected and dried over $CaCl_2$. Remaining solvent was removed after which vacuum distillation (∼105 °C, 2.5 Torr) yielded a clear colorless air sensitive oil in a yield of 30%.

$Cu_{2-x}Se$ QDs Synthesis. $Cu_{2-x}Se$ QDs were synthesized following an adaptation of a previously reported method for the synthesis of $Cu_{2-x}S$ NSs.[28] The main adaptations were the use of DDSe instead of DDT, a lower reaction temperature, and a shorter reaction time. Typically, 0.22 mmol of Cu(OAc), and 0.075 mmol of $SnBr_4$ were mixed with 12.5 mL of ODE and 0.55 g of TOPO. The mixture was degassed for 30 min at 100 °C under vacuum. The solution was then heated to 130 °C, and 0.6 mL of DDSe was swiftly injected, the reaction mixture being still under vacuum. Directly after the injection, the reaction solution turned clear yellow/orange and was purged with a N_2 gas flow. The temperature was further increased to 170 °C, and the reaction mixture turned turbid brown/black at ∼150 °C. The solution was maintained at 170 °C for 15 min and was then cooled to RT by removing the heating mantle. The $Cu_{2-x}Se$ NCs were precipitated by adding a 1:1 methanol:butanol solution, followed by centrifugation. The supernatant was discarded and the NCs were dispersed in ∼2 mL of toluene. These washing steps were repeated three times.

$Cu_{2-x}Se$ Nanoplatelet Synthesis. A modification of the method described above to synthesize $Cu_{2-x}Se$ QDs was used to synthesize $Cu_{2-x}Se$ nanoplatelets. Typically, 31.6 mg (0.22 mmol) of CuBr and 30.8 mg (0.30 mmol) of NaBr were mixed with 12.5 mL ODE and 0.55 g of TOPO. After degassing for 30 min at 100 °C, the solution was heated to 130 °C, and 0.6 mL of DDSe was swiftly injected, all under vacuum. After the injection, the reaction mixture was purged with a N_2 gas flow, and the temperature was further increased to 170 °C. The solution was maintained at 170 °C for 40 min and was then cooled to RT by removing the heating mantle. The $Cu_{2-x}Se$ NCs were precipitated by adding a 1:1 methanol:butanol solution, followed by centrifugation. The supernatant was discarded, and the NCs were dispersed in ∼2 mL of toluene. These washing steps were repeated three times. The aspect ratio of the platelets (thicker and smaller lateral dimensions) can be tuned by using 0.22 mmol of Cu(OAc), 0.075 mmol of $SnCl_4{\cdot}5H_2O$, 12.5 mL of ODE, and 0.55 g of TOPO.

$Cu_{2-x}Se$ NSs Synthesis. $Cu_{2-x}Se$ NSs were synthesized following an adaptation of the protocol described above to synthesize the $Cu_{2-x}Se$ QDs. Typically, 15.8 mg (0.11 mmol) of CuBr and 15.4 mg (0.15 mmol) of NaBr were mixed with 6.25 mL of ODE. After degassing for 30 min at 100 °C, the solution was heated to 130 °C, and 0.25 mL of DDSe was swiftly injected, all under vacuum. After the injection, the reaction mixture was purged with a N_2 gas flow, and the temperature was further increased to 170 °C. The solution was maintained at 170 °C for 40 min and was then cooled to RT by removing the heating mantle. The $Cu_{2-x}Se$ NSs were precipitated by adding a 1:1 methanol:butanol solution, followed by centrifugation. The supernatant was discarded and the NCs were dispersed in ∼2 mL of toluene.

Control Experiment. In the experiment used to investigate the influence of halide ions present in solution, the synthesis for $Cu_{2-x}Se$

DOI: 10.1021/acs.chemmater.8b01143
Chem. Mater. 2018, 30, 3836−3846

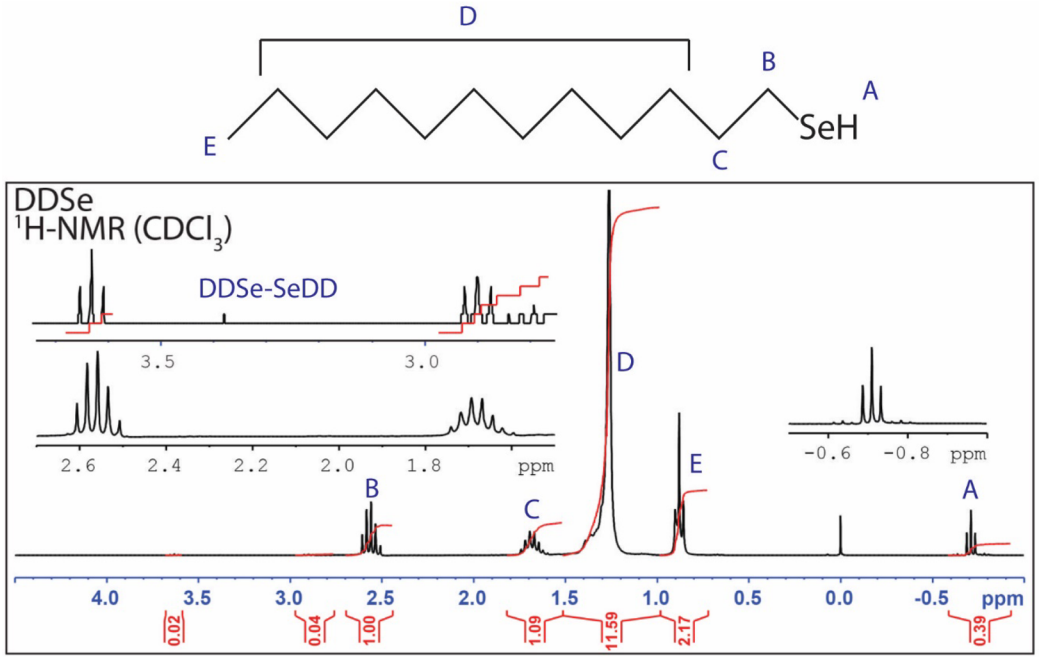

Figure 1. [1]H NMR spectrum of synthesized DDSe, with the integrals in red below the peaks. The letters indicate the chemically different protons that can be distinguished in the NMR spectrum. The insets show enlarged regions of the spectrum.

quantum dots was performed as ascribed above, however without the addition of Br^- salt.

Cation Exchange to CdSe. A 0.06 M Cd-stock solution was prepared by dissolving 0.08 g (0.4 mmol) $CdCl_2$ in 7 mL of methanol. 0.5 mL of $Cu_{2-x}Se$ NCs in toluene (as prepared above) was mixed with 0.5 mL of Cd-stock solution and 50 μL of TOP and left at room temperature for approximately 24 h. The color of the NC solutions changed to red immediately after addition of the Cd-stock solution and TOP. Prior to TEM and elemental analysis, the NCs were washed with methanol and redispersed in toluene.

Partial Cation Exchange to $CuInSe_2$. An In-stock mixture was prepared by mixing 0.22 g (1 mmol) of $InCl_3$ in 3 mL of ODE and 0.5 mL (1 mmol) of TOP. This mixture was heated at a heating plate set at 180 °C while stirring for 30 min. 0.5 mL of $Cu_{2-x}Se$ NCs in toluene (as prepared above) was mixed with 40 μL of In-stock mixture and placed at a heating plate with a temperature set at 100 °C overnight. Prior to TEM and elemental analysis, the NCs were washed with methanol and redispersed in toluene.

Electron Microscopy. Transmission electron microscopy (TEM) and electron diffraction measurements were performed on a FEI Tecnai 10, 12 or 20-FEG microscope. Samples were prepared by drop-casting a NC solution in toluene on a carbon-coated copper grid. Azimuthal integration with CrystBox[29] was used to analyze the electron diffraction patterns. Energy dispersive X-ray spectroscopy (EDS) experiments were performed on a FEI Tecnai 20-FEG or FEI Talos F200X microscope, using carbon-coated aluminum grids.

X-ray Diffraction (XRD). Diffraction measurements were performed with a Bruker D2 Phaser equipped with a Co Kα X-ray source with X-ray wavelength of 1.79026 Å. Thin solid film NC samples for XRD were prepared by drop-casting a concentrated NC solution in chloroform on a Si wafer and evaporating the solvent.

Absorption and Photoluminescence Spectroscopy. Absorption spectra were measured on a double-beam PerkinElmer Lambda 950 UV/vis spectrophotometer. NC solutions were measured in toluene and stored in sealed quartz cuvettes. Photoluminescence (PL) and PL excitation spectra were measured on an Edinburgh Instruments FLS920 spectrofluorometer equipped with a Hamamatsu R928 detector with a monochromator grated at 500 nm or a Hamamatsu R5509-72 PMT with a monochromator grated at 1200 nm. A 900 W Xe lamp was used as excitation source.

Time-Resolved PL Spectroscopy. Samples for time-resolved PL spectroscopy were prepared by diluting the stock solution of washed NCs with anhydrous toluene under nitrogen and stored in sealed quartz cuvettes. PL decay curves were obtained by time-correlated single-photon counting on a Hamamatsu photosensor module R5509-72. A pulsed diode laser was used as the excitation source: EPL-445 Edinburgh Instruments, 441 nm, 55 ps pulse width, 0.2 MHz repetition rate. Lifetimes were obtained from a biexponential fit of the decay curve.

Model Visualization. Panels A–F in Figure 6 were made using the program Vesta.[30]

RESULTS AND DISCUSSION

Dodecaneselenol. After synthesis and purification (see Experimental Section for details), a very light yellow colored liquid product was obtained, which was analyzed by proton nuclear magnetic resonance ([1]H NMR, Figure 1). The majority of the peaks observed in the [1]H NMR spectrum can be assigned to the desired product 1-dodecaneselenol (DDSe),[31,32] but peaks due to impurities (DDSe–DDSe and dodecane, DDH) are also present (see Supporting Information for details concerning the assignment). The purity of the product dodecaneselenol can be calculated by comparing the peaks at 1.5–1.2 ppm (DDSe + DDSe-SeDD + DDH), the peak at 2.58 ppm (DDSe + DDSe-SeDD), and the peak at 3.62 ppm (DDSe-SeDD), which indicates that the product consists of 76% DDSe, 22% DDH, and 2% DDSe-SeDD. The reaction yield was 30%. As the main impurity was dodecane, which should not influence the NC synthesis since it contains no Se and is noncoordinating, no further purification steps than described in the Experimental Section were performed. A [13]C NMR spectrum of the product mixture is shown in the Supporting Information (Figure S1). The DDSe was stored under inert atmosphere and in the dark, as oxygen and light induce oxidation to the more stable diselenide (DDSe-SeDD) (Figure S2).

DDSe as Se-Precursor in the Synthesis of Colloidal $Cu_{2-x}Se$ NCs. To verify the adequacy of the as-prepared DDSe

DOI: 10.1021/acs.chemmater.8b01143
Chem. Mater. 2018, 30, 3836–3846

as Se-precursor for the preparation of colloidal $Cu_{2-x}Se$ NCs, we adapted a previously published synthesis protocol for $Cu_{2-x}S$ NCs[28] by simply replacing DDT by DDSe (0.6 mL of DDSe was injected into a solution of 0.22 mmol of Cu(OAc), 0.075 mmol of $SnBr_4$, and 0.55 g of TOPO in 12.5 mL of ODE at 160 °C, followed by heating up to 220 °C and 40 min of reaction). To allow the direct comparison of the reactivity of both precursors, we intentionally kept all reaction parameters the same. One minute after DDSe injection, a sample was taken and analyzed with X-ray diffraction (XRD), transmission electron microscopy (TEM), and optical spectroscopy (see Figure S3). The low angle X-ray diffractogram (Figure S3A) shows periodic peaks, spaced by 3.7 nm, similar to those observed for lamellar Cu−thiolate complexes[33] that are observed at early stages of the $Cu_{2-x}S$ NCs synthesis using DDT as sulfur precursor.[23,28] The XRD patterns of the Cu-DDSe and Cu-DDT complexes are essentially identical, both in peak position and in relative peak intensity. This is not unexpected since the atomic radii of S^{2-} and Se^{2-} only differ by 13 pm,[34] and therefore the differences in the lamellae thickness due to the chalcogen atoms cannot be distinguished in XRD patterns. TEM analysis of the sample obtained after 1 min reveals thin rectangular sheets (Figure S4) that disappear as the reaction proceeds and are thus attributed to Cu-DDSe lamellar complexes formed in situ following the injection of DDSe in the hot reaction mixture. This assignment is supported by the absorption and PL spectra of the sample extracted 1 min after injection (Figure S3B), which revealed features similar to those previously observed for Br-stabilized Cu-DDT lamellar complexes.[28] It is thus likely that Br-stabilized Cu-DDSe lamellar complexes are also formed at early reaction stages. The differences between the optical properties of the Cu-DDT and Cu-DDSe lamellar complexes can be understood by considering the intrinsic characteristics of ligand-to-metal charge-transfer transitions involving S and Se, respectively (see the Supporting Information for a detailed discussion).

This exploratory $Cu_{2-x}Se$ NC synthesis yielded polydisperse NCs (Figure 2A and Figure S5A), in striking contrast with the ultrathin $Cu_{2-x}S$ nanosheets (NSs) that are obtained in the DDT-based synthesis under the same reaction conditions.[28] We attribute the morphological differences between the $Cu_{2-x}S$ and the $Cu_{2-x}Se$ product NCs to the combined effects of a weaker Se−C bond and a lower thermal stability of the lamellar Cu-DDSe complexes, in comparison to the sulfide analogues. The latter results in the formation of an isotropic phase before the nucleation threshold of $Cu_{2-x}Se$ NCs can be overcome, thereby preventing the formation of 2D NCs by soft templating effects, in contrast to the Cu-DDT-based synthesis.[23,28] In the Cu-DDT system, halide ions were shown to increase the thermal stability of the lamellar Cu-DDT complexes, allowing them to stay intact at temperatures that were sufficiently high for nucleation and growth of $Cu_{2-x}S$ NCs, thereby promoting the formation of 2D nanosheets.[23] However, in the present study the stabilization effect of the Br^- ions appears to be too weak to impose 2D constraints on the nucleation and growth of $Cu_{2-x}Se$ NCs, under the reaction conditions used. Moreover, the weaker Se−C bond results in lower activation energies for thermolysis of the Cu-DDSe complexes, thereby forming [CuSe] monomers at lower temperatures and at faster rates, leading to faster growth rates than those observed for the sulfide analogues at the same temperatures.

Colloidal $Cu_{2-x}Se$ NCs with Narrow Size and Shape Dispersion. The exploratory experiments described above clearly demonstrate that the controlled synthesis of $Cu_{2-x}Se$ NCs using DDSe as chalcogen precursor requires milder reaction conditions than those used in the synthesis of colloidal $Cu_{2-x}S$ NCs using DDT. Indeed, lower injection and growth temperatures (130 and 170 °C instead of 160 and 220 °C, respectively) improved the size and shape control but did not restore the 2D contraints, yielding quantum dots with a diameter (d) of 4.9 ± 0.5 nm after 15 min of reaction (see Figure 2B). The formation of 2D NCs (nanoplatelets with a thickness h of 4.4 ± 0.6 nm and lateral dimensions l of 21 ± 6 nm) required not only longer reaction times (40 min) but also the replacement of Cu(OAc) and $SnBr_4$ by CuBr and NaBr (Figure 2C) (i.e., higher Br concentrations). The use of NaBr

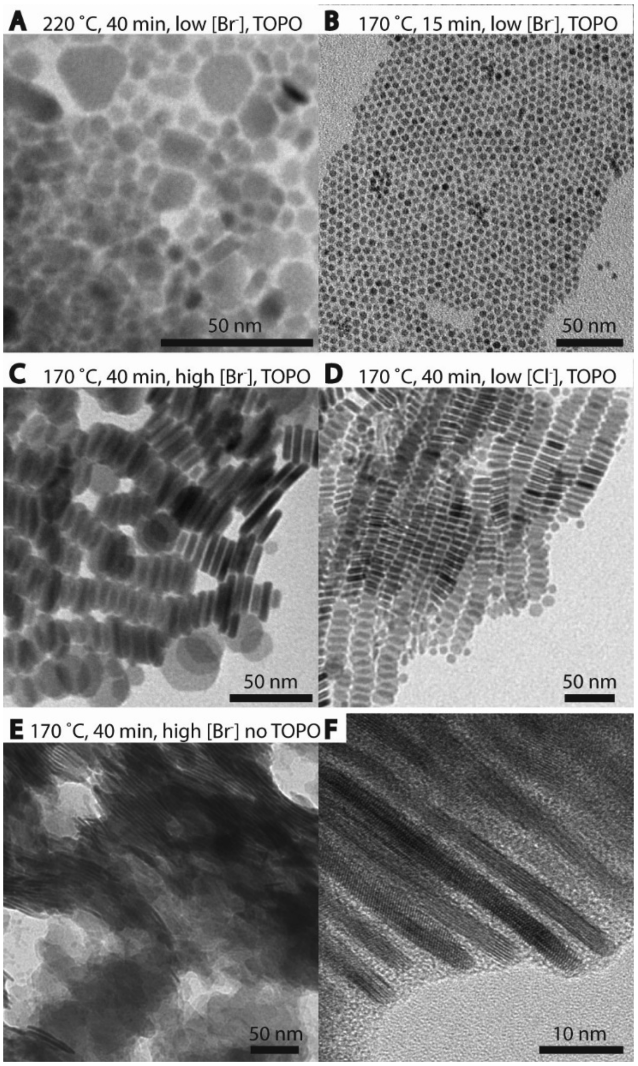

Figure 2. TEM images of $Cu_{2-x}Se$ NCs with different aspect ratios. The corresponding size histograms are shown in Figure S5. (A) $Cu_{2-x}Se$ NC sample obtained after 40 min reaction at 220 °C, using Cu(OAc), $SnBr_4$ and TOPO. (B) $Cu_{2-x}Se$ quantum dots (d = 4.9 ± 0.5 nm) obtained after 15 min reaction at 170 °C, using Cu(OAc), $SnBr_4$, and TOPO. (C) $Cu_{2-x}Se$ platelets (h = 4.4 ± 0.6 nm, l = 21 ± 6 nm) obtained after 40 min reaction at 170 °C, using CuBr, NaBr, and TOPO. (D) $Cu_{2-x}Se$ platelets (h = 7.0 ± 0.5 nm, l = 17 ± 2 nm) obtained after 40 min reaction at 170 °C, using Cu(OAc), $SnCl_4{\cdot}H_2O$, and TOPO. (E) Stacked and flat lying $Cu_{2-x}Se$ NSs (h = 2.4 ± 0.4 nm) obtained after 40 min reaction at 170 °C, using CuBr and NaBr, without TOPO. (F) HR-TEM image of stacked NSs (additional and larger size images are shown in Figure S6).

DOI: 10.1021/acs.chemmater.8b01143
Chem. Mater. 2018, 30, 3836−3846

instead of $SnBr_4$ to achieve higher concentrations of Br is motivated by the fact that high concentrations of $SnBr_4$ have been shown to affect the nucleation and growth rates of $Cu_{2-x}S$ NCs synthesized using the sulfur-analogue DDT.[24] Addition of chloride ions ($SnCl_4 \cdot 5H_2O$) to the reaction mixture (see the Experimental Section for details) led to nanoplatelets with a lower aspect ratio ($h = 7.0 \pm 0.5$ nm, $l = 17 \pm 2$ nm) than those obtained with bromide addition (Figure 2D). Ultrathin $Cu_{2-x}Se$ NSs ($h = 2.4 \pm 0.4$ nm) were synthesized by carrying out the reaction in the absence of TOPO, while keeping CuBr as Cu(I) precursor and NaBr as Br source and a low reaction temperature (Figure 2E,F). The lateral dimensions of the NSs range from ~50 to ~100 nm (Figure 2E), and their thickness is around 4 monolayers with a spacing of 0.78 nm, as shown in high-resolution (HR) TEM images (Figure 2F and Figure S6). Size histograms of the $Cu_{2-x}Se$ NCs discussed in this section are shown in the Supporting Information (Figure S5). A control experiment without halides and using Cu(I) acetate as precursor confirms the stabilizing effect of halide ions, as the NCs obtained under these conditions have very low aspect ratios (Figure S7). The similarity between the shape-directing abilities of Cu(I)-DDSe complexes and those of Cu(I)-DDT complexes implies that the synthesis of colloidal $Cu_{2-x}Se$ NCs using DDSe as Se-precursor is capable of reaching the same level of mastery already demonstrated for the synthesis of colloidal $Cu_{2-x}S$ NCs using DDT as S-precursor.[1,2,23,24] Moreover, the insights revealed by our work are likely applicable also to the direct synthesis of shape-controlled NCs of other metal selenides, since selenolate complexes of several metals are known (e.g., Ag(I), Sn(II), Pb(II), and In(III)),[25,26] and DDSe may thus be able to form lamellar complexes with a variety of other metals.

Postsynthetic Cation Exchange Conversion of $Cu_{2-x}Se$ Template NCs to CdSe and $CuInSe_2$ NCs. $Cu_{2-x}Se$ NCs with three different morphologies (dots, platelets, and sheets; see Figure 2B,D,E, respectively, for representative examples) were used as templates in cation exchange (CE) reactions (see Experimental Section for details). The optical spectra of the template and product NCs are shown in Figure 3 and Figure S8. The dimensions of these NCs will be discussed below (Figure 4) in more detail. The template $Cu_{2-x}Se$ quantum dots, nanoplatelets, and nanosheets show a strong and featureless absorption in the UV−vis region of the spectrum accompanied by a broad band in the NIR. The absorption spectrum of the $Cu_{2-x}Se$ quantum dots shows also a small peak at 360 nm, which is ascribed to residual Cu-DDSe complexes, since this peak is already observed immediately after the DDSe injection and becomes gradually weaker as the growth proceeds. NIR absorption bands similar to those displayed in the spectra of the template $Cu_{2-x}Se$ NCs (Figure 3) are commonly observed for Cu-chalcogenide NCs and have been ascribed to localized surface plasmon resonances due to excess charge carriers (typically valence band holes originating from Cu vacancies).[1,2,35] The NIR absorption bands are no longer present in the absorption spectra of the product NCs obtained from the CE reactions, indicating the absence of Cu vacancies and the successful conversion of the template $Cu_{2-x}Se$ NCs into either CdSe or $CuInSe_2$ NCs, through Cu^+ for Cd^{2+} or partial, self-limited Cu^+ for In^{3+} CE, respectively.

The absorption spectra of the CdSe NCs (quantum dots, nanoplatelets, and nanosheets) show well-defined features that can be ascribed to the lowest energy transitions of quantum confined excitons. These features are better defined in the

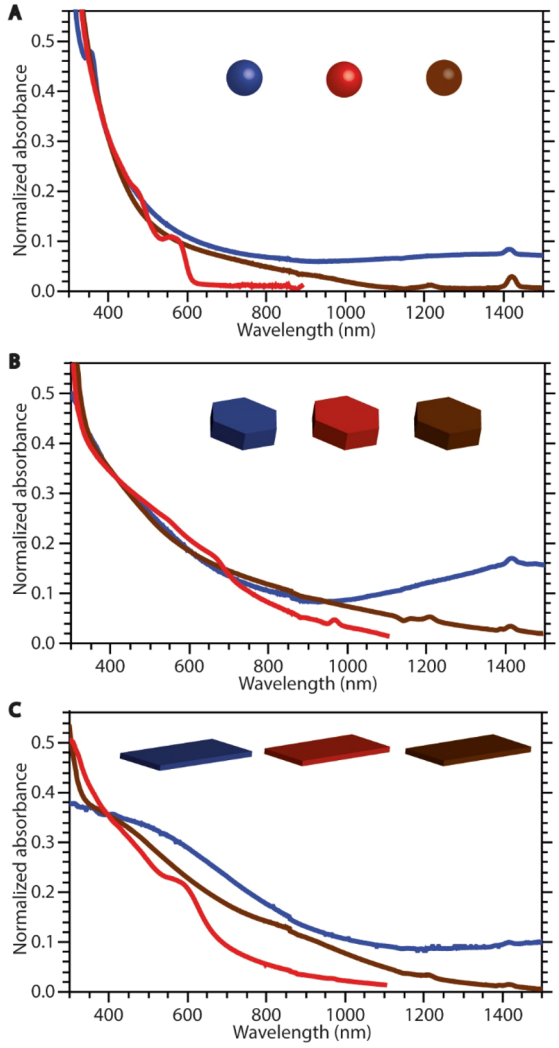

Figure 3. Absorption spectra of template $Cu_{2-x}Se$ NCs (blue lines) and product CdSe NCs (red lines) and $CuInSe_2$ NCs (brown lines) obtained after CE reactions (Cu^+ for Cd^{2+}, and partial, self-limited Cu^+ for In^{3+}, respectively). The spectra were normalized at 400 nm. TEM images of the samples used to acquire the optical spectra are shown below (Figure 4). (A) Absorption spectra of quantum dots of different compositions. (B) Absorption spectra of thick nanoplatelets. Optical spectra of thinner ($l \leq 4.2$ nm) CdSe nanoplatelets displaying PL are shown in Figure S11. (C) Absorption spectra of ultrathin nanosheets.

spectrum of the CdSe QDs and are consistent with the $1S_{3/2(h)} \rightarrow 1S_{(e)}$, $2S_{3/2(h)} \rightarrow 1S_{(e)}$ and $1P_{(h)} \rightarrow 1P_{(e)}$ transitions of CdSe QDs with an ~4 nm diameter.[36,37] The peak positions in the absorption spectra of the CdSe nanoplatelets and nanosheets are also consistent with their thicknesses (their dimensions will be discussed in more detail below) but are partially distorted by the presence of a light scattering background, since these NCs tend to forms stacks (see below for details). The absorption spectra of the product $CuInSe_2$ NCs do not show well-defined features, regardless of the NC shape (Figure 3). The product $CuInSe_2$ QDs show PL in the NIR, characterized by a large global Stokes shift and slow PL decay times (Figure S9). These optical characteristics are typical for NCs of ternary copper indium chalcogenides.[1,38−41]

The PL of the product CdSe QDs and nanosheets is strongly red-shifted with respect to the lowest energy absorption transition, very broad, and slow decaying (see Figures S8 and

DOI: 10.1021/acs.chemmater.8b01143
Chem. Mater. 2018, 30, 3836−3846

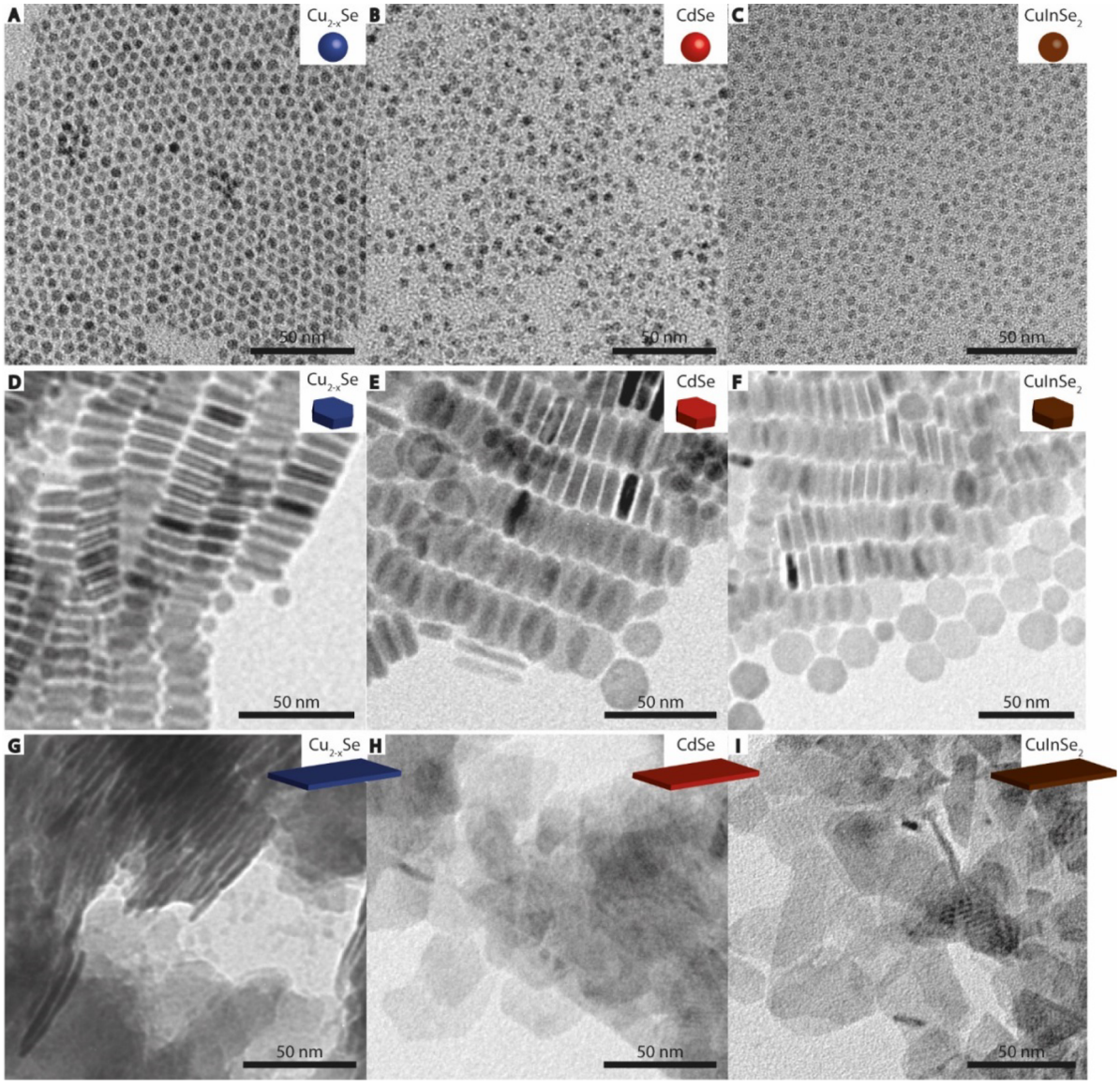

Figure 4. TEM images of (A) template $Cu_{2-x}Se$ quantum dots, $d = 4.9 \pm 0.5$ nm. (B) Product CdSe quantum dots with $d = 4.1 \pm 0.7$ nm, obtained by Cu^+ for Cd^{2+} cation exchange using the NCs shown in (A) as templates. (C) Product $CuInSe_2$ quantum dots with $d = 3.6 \pm 0.7$ nm, obtained by partial Cu^+ for In^{3+} cation exchange using the NCs shown in (A) as templates. (D) Template $Cu_{2-x}Se$ nanoplatelets ($h = 7.0 \pm 0.5$ nm, $l = 17 \pm 2$ nm). (E) Product CdSe nanoplatelets with $h = 6.0 \pm 0.7$ nm and $l = 21 \pm 3$ nm, obtained by Cu^+ for Cd^{2+} cation exchange using the NCs shown in (D) as templates. (F) Product $CuInSe_2$ nanoplatelets ($h = 4.9 \pm 0.7$ nm, $l = 21 \pm 1$ nm) obtained by partial Cu^+ for In^{3+} cation exchange using the NCs shown in (D) as templates. (G) Template ultrathin $Cu_{2-x}Se$ nanosheets ($h = 2.4 \pm 0.4$ nm, $l = 50-100$ nm). (H) Product ultrathin CdSe nanosheets obtained by Cu^+ for Cd^{2+} cation exchange using the NCs shown in (G) as templates. (I) Product $CuInSe_2$ nanosheets obtained by partial Cu^+ for In^{3+} cation exchange using the NCs shown in (G) as templates. All scale bars correspond to 50 nm.

S9). These observations suggest Cu^+-dopant mediated radiative decay, as shown before for Cu^+:CdSe QDs[42,43] and nanosheets.[44] Low Cu concentrations were indeed detected with EDX analysis in the product CdSe NCs (~0.5% in the dots and ~2% in the nanoplatelets and nanosheets, see Figure S10). This is an indication that the Cu^+ for Cd^{2+} CE was not complete. EDX analysis of the $CuInSe_2$ NC samples yielded a Cu:In ratio of 1:2 (see Figure S10). However, the possibility that these samples contained residual indium precursor cannot be excluded.

Figure 4 shows TEM images of the template $Cu_{2-x}Se$ NCs and of the product CdSe and $CuInSe_2$ NCs obtained after CE reactions. It is clear that the shape of the template NCs is preserved after the CE reaction, thus making ultrathin $CuInSe_2$ nanosheets accessible for the first time and also hexagonal CdSe nanoplatelets. Nevertheless, the cation exchange was not truly topotactic, since the dimensions of the product NCs were slightly altered with respect to those of the template NCs. In the case of the dot-shaped NCs, the dimensions changed from $d_{Cu_{2-x}Se} = 4.9 \pm 0.5$ nm to $d_{CdSe} = 4.1 \pm 0.7$ nm and $d_{CuInSe_2} = 3.6 \pm 0.7$ nm, while for the nanoplatelets they changed from $h = 7.0 \pm 0.5$ nm, $l = 17 \pm 2$ nm for the parent $Cu_{2-x}Se$ NCs to $h = 6.0 \pm 0.7$ nm, $l = 21 \pm 3$ nm for the CdSe nanoplatelets and $h = 4.9 \pm 0.7$ nm, $l = 21 \pm 1$ nm for the $CuInSe_2$ nanoplatelets (see Figure S12 for the corresponding size histograms). The decrease in size of the dot-shaped NCs after the CE reactions is ascribed to etching, as the TEM images (Figure 4E,I) show irregularly shaped NCs, in contrast to the template $Cu_{2-x}Se$

DOI: 10.1021/acs.chemmater.8b01143
Chem. Mater. 2018, 30, 3836−3846

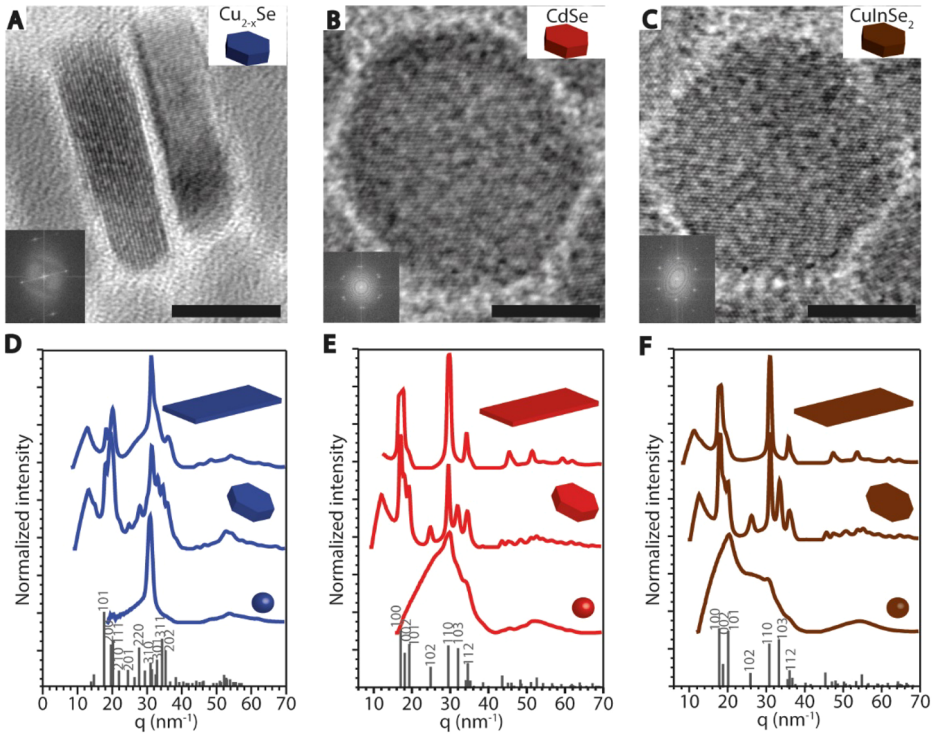

Figure 5. HR-TEM images of (A) template $Cu_{2-x}Se$ nanoplatelets. (B) Product CdSe nanoplatelets obtained by Cu^+ for Cd^{2+} cation exchange using the NCs shown in (A) as templates. (C) Product $CuInSe_2$ nanoplatelets obtained by partial Cu^+ for In^{3+} cation exchange using the NCs shown in (A) as templates. All scale bars correspond to 10 nm. In the images of the CdSe and $CuInSe_2$ nanoplatelets, the hexagonal lattice can be recognized. The insets show the FFT of the images that were used to determine the lattice spacings. Azimuthally integrated ED ring patterns of all three morphologies of (D). Template $Cu_{2-x}Se$ NCs. (E) Product CdSe NCs. (F) Product $CuInSe_2$ NCs. Bulk XRD reference patterns for umangite (D, JPCDS PFD card 00-047-1745), wurtzite (E, JPCDS PFD card 04-011-9600), and hexagonal $CuInSe_2$ (F, JPCDS PFD card 01-078-5190) are also shown. The ED ring patterns are shown in Figures S13–S15.

dot-shaped NCs (Figure 4A). The lateral dimensions of the nanoplatelets increased after the CE reaction, while the thickness decreased. This is ascribed to an internal reconstruction and ripening process accompanying a change in crystal structure and will be discussed in more detail below. The nanosheets no longer formed stacks after the CE, and therefore their thickness could not be determined.

HR-TEM imaging and electron diffraction (ED) experiments were performed on the set of three differently shaped NCs, before and after CE (Figure 5 and Figures S13–S15). Figure 5A shows a HR-TEM image of $Cu_{2-x}Se$ nanoplatelets, with some nanoplatelets oriented such that lattice fringes can be observed. A fast Fourier transform (FFT) of this image allows the measurement of the lattice spacings in these $Cu_{2-x}Se$ nanoplatelets, yielding 0.11, 0.17, and 0.45 nm. Azimuthal integration of the ED ring patterns yields signals that can be compared to bulk X-ray powder diffraction (XRD) reference patterns, as shown in Figures 5D–F. The diffraction patterns of the different morphologies are not identical, most likely due to the limited number of lattice planes in the ultrathin nanosheets and dots and the different orientation of the nanoplatelets and nanosheets on the TEM grid (nanosheets are mostly lying flat on the large facets, while the nanoplatelets are mostly ordered in stacks oriented perpendicular to the large facets). However, the peaks in the diffraction patterns of the nanosheets coincide with the main peaks in the diffraction patterns of the nanoplatelets, and we thus assume that these differently shaped NCs have the same crystal structure. The ED patterns of the dots are rather featureless, which can be explained by peak broadening due to their small size (visible as diffuse gray values in the measured ring patterns; see Figures S13A, S14A, and S15A). The presence of a strong peak in the ED pattern of the $Cu_{2-x}Se$ dots (Figure 5D) is intriguing and suggests that the self-organized hexagonal superlattice formed by these NCs on the TEM grid (Figure S13A) may have a preferred orientation. The absence of peaks at q-values lower than ~20 is due to the e-beam stopper that blocks the intense signal close to the center, which is necessary to enhance the contrast at larger q-values (see Figures S13A, S14A, and S15A).

The ED pattern of the $Cu_{2-x}Se$ nanoplatelets matches the tetragonal umangite XRD reference pattern (JPCDS PFD card 00-047-1745, Figure 5D and Figure S16). A comparison with other crystal structures known for $Cu_{2-x}Se$ was made, but none of these gave a better match than the umangite reference (see Figure S17). We assume that all three morphologies have the same crystal structure. In the following, we will focus on the nanoplatelets, which yielded a more complete data set. After conversion of the template $Cu_{2-x}Se$ NCs to CdSe NCs by CE, a hexagonal crystal lattice is obtained, as clearly shown in the HR-TEM images and corresponding FFTs (Figure 5B and Figure S14). The lattice spacings determined are 0.18 and 0.10 nm. The ED pattern of the nanoplatelets corresponds very well with the wurtzite CdSe reference JPCDS PFD card 04-011-9600 (Figure 5E). The highest intensity peaks correspond to the (100) and (110) planes, indicating that the top facet is the (002) plane, similar to the wurtzite CdSe nanoplatelets reported earlier.[45] In the HR-TEM image and FFT of the product $CuInSe_2$ nanoplatelets obtained by CE, a hexagonal pattern is also recognized, with lattice spacings of 0.17 and 0.10 nm (Figure 5C and Figure S15). The ED pattern of the

DOI: 10.1021/acs.chemmater.8b01143
Chem. Mater. 2018, 30, 3836–3846

$CuInSe_2$ nanoplatelets corresponds very well to the hexagonal $CuInSe_2$ XRD reference JPCDS PFD card 01-078-5190. We assume this crystal structure for all the product $CuInSe_2$ NCs. Furthermore, we infer that the product $CuInSe_2$ NCs have the same faceting as the product CdSe NCs, since the position and relative intensities of the reflections are similar (compare Figures 5E and 5F). It is interesting to note that the direct transformation of copper selenide to $CuInSe_2$ has also been observed by solid-state reaction between $CuSe_2$ and elemental indium powders promoted by high-energy mechanical milling.[46] However, in this case, the reaction involves the simultaneous oxidation of In^0 to In^{3+} and reduction of Cu^{2+} to Cu^+ and of Se_2^{2-} to Se^{2-},[46] in contrast with the present work, which does not involve any redox reactions, since Cu is already in its +1 oxidation state in $Cu_{2-x}Se$ and In is already in the +3 oxidation state in the precursor used for the CE reaction. Moreover, the solid-state transformation reported in ref 46 results in tetragonal $CuInSe_2$, while hexagonal $CuInSe_2$ is obtained in the present work.

Mechanism for the NC Reconstruction during the Cation Exchange. As shown above, the tetragonal crystal structure of the template $Cu_{2-x}Se$ NCs changes to a hexagonal structure in the product CdSe and $CuInSe_2$ NCs. This structural transformation is accompanied by a reconstruction of the NC, through which its overall shape is preserved despite changes in its aspect ratio (i.e., the thickness decreases, while the lateral dimensions increase). This is unusual, as CE reactions are typically topotactic, leaving the anionic sublattice undisturbed, thereby preserving the size, shape, and anionic sublattice structure of the template NCs in the product NCs.[4−7,47] Very few examples of reorganization of the anionic sublattice during CE reactions are known, viz. the transformation of trigonal In_2S_3 NCs to tetragonal $CuInSe_2$ NCs in water,[48] covellite CuS NCs to wurtzite CdS NCs,[49] and hexagonal Cu_2Te nanodisks to wurtzite CdTe nanodisks.[18] In the latter case, the main anionic displacement is in the *z*-direction with an average displacement of 0.19 nm per Te atom (based on unit cell parameters) which leads to tilting of the *c*-axis (the [001] direction) by 90°, from perpendicular to the nanodisk plane to in-plane.[18] Modeling of both unit cells predicted an overall compression of the in-plane area of 5% and an increase in thickness of 25%, in good agreement with the observed increase in thickness of 22% for the product CdTe disks.[18]

The unit cell dimensions of the systems we discuss here are very similar to each other, however in different orientations: tetragonal umangite has $a = b = 0.640$ nm and $c = 0.428$ nm (JPCDS PFD card 00-047-1745), while hexagonal wurtzite CdSe has $a = b = 0.426$ nm and $c = 0.695$ nm (JPCDS PFD card 04-011-9600). Calculations based on these values yield an expected increase in lateral dimensions of 7.9% (0.06 nm per unit cell) and a decrease in thickness of 0.5% (0.002 nm per unit cell). However, from the different views on slabs of umangite and wurtzite in Figure 6, it is clear that the anionic sublattices in umangite and wurtzite are not equivalent. This means that upon conversion of umangite to wurtzite by either Cu^+ for Cd^{2+} or partial Cu^+ for In^{3+} CE, not only the dimensions of the unit cells should change but also the anionic sublattice itself should undergo reconstruction. Figure 6G shows a 3-dimensional model superposing the anionic sublattices of umangite and wurtzite. From this model, it is clear that conversion of the template umangite NCs to product wurtzite NCs requires expansion in all three dimensions (viz., 16% in the *x*−*y* plane and 10% in the *z*-direction), leading to an overall increase in volume of 29%.

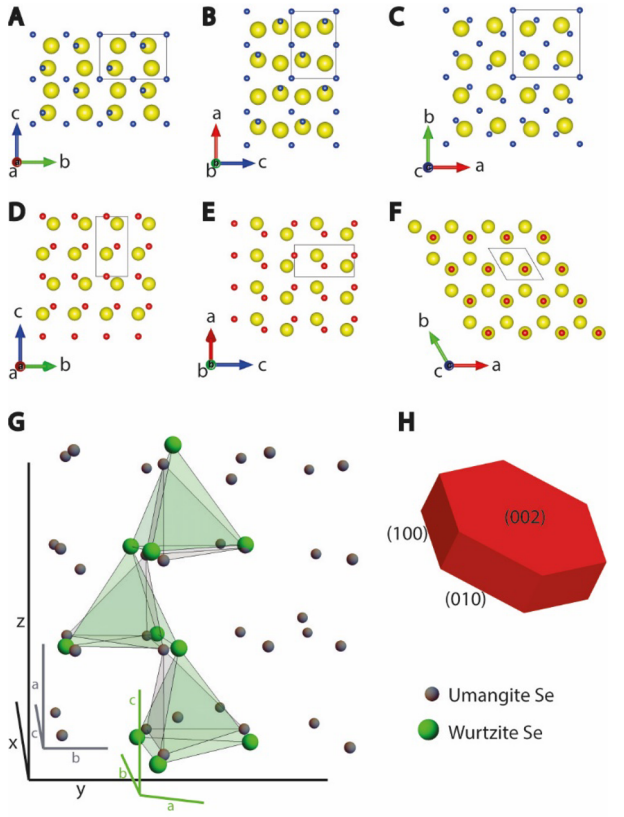

Figure 6. (A−C) Schematic views of Cu_3Se_2 umangite slabs, with the unit cell indicated. Selenium anions are displayed in yellow and copper cations in blue. (D−F) Schematic views of CdSe wurtzite slabs with the unit cell indicated. Selenium anions are displayed in yellow and cadmium cations in red. (G) Three-dimensional model of the umangite (gray) and wurtzite (green) anionic sublattice. The *a*, *b*, *c* directions of the unit cells are indicated. For convenience general *x*, *y*, *z* directions are indicated in black. (H) Schematic representation of wurtzite nanoplatelet, with facets indexed.

The experimentally observed dimensions of the nanoplatelets are thickness $h = 7.0 \pm 0.5$ nm and diameter $l = 17 \pm 2$ nm for the template umangite $Cu_{2-x}Se$ NCs, $h = 6.0 \pm 0.7$ nm and $l = 21 \pm 3$ nm for the product wurtzite CdSe NCs, and $h = 4.9 \pm 0.7$ nm and $l = 21 \pm 1$ nm for the product $CuInSe_2$ NCs (Figure 4). This corresponds to an increase in lateral dimensions of 23.5 ± 0.2% and 23.5 ± 0.1% and a decrease in thickness of 14.3 ± 0.1% and 30.0 ± 0.1% for the CdSe and $CuInSe_2$ NCs, respectively. It is interesting to note that this in striking contrast with the expectations based on the calculations above, since the observed expansion in the *xy*-plane is much larger than that expected (23.5% instead of 16%), while a contraction in the *z*-direction (by 14.3% and 30% for CdSe and $CuInSe_2$, respectively) is observed instead of the expected expansion of 10%. In terms of the overall volume, the CdSe nanoplatelets expand by 26.4 ± 0.3% (assuming a perfect hexagonal prism with height $h = 6.0 \pm 0.7$ nm, side length $s = 10.8 \pm 0.9$ nm, and apothem $a = 11 \pm 1$ nm), while the $CuInSe_2$ nanoplatelets expand by only 7.4 ± 0.3% (assuming a perfect hexagonal prism with $h = 4.9 \pm 0.7$ nm, $s = 11.6 \pm 1$ nm, and $a = 10.6 \pm 0.7$ nm) in comparison to the template $Cu_{2-x}Se$ nanoplatelets (assuming a perfect hexagonal prism $h = 7.0 \pm 0.5$ nm, $s = 9 \pm 1$ nm, and $a = 8 \pm 1$ nm). The overall

DOI: 10.1021/acs.chemmater.8b01143
Chem. Mater. 2018, 30, 3836−3846

expansion of the CdSe nanoplatelets is only slightly smaller than that expected (26.4% instead of 29%), suggesting that the larger expansion in the lateral direction occurred to compensate for the reduction in thickness. However, the expansion of the $CuInSe_2$ nanoplatelets (7.4%) is significantly smaller than that expected, mostly because the expansion in the *xy*-direction was not enough to compensate the pronounced contraction in the *z*-direction.

These observations indicate that the observed reconstruction of the product NCs is driven not only by the reorganization of the anionic sublattice that is required for the structural transformation from tetragonal umangite to hexagonal wurtzite but also by internal ripening processes that favor extension of the lateral dimensions at the expenses of the thickness. The process of internal ripening, where elemental units move from high-energy facets to low-energy facets, has been observed before for many different NC systems and typically results in reduction of the anisotropy of the NC shape (e.g., nanorods become shorter and thicker).[13] It is known that the polar facets of wurtzite CdSe have a higher free energy and are generally less densely passivated by ligands (e.g., alkylamines or alkylphosphonic acids) than the nonpolar facets[50] and therefore tend to be eliminated when internal ripening processes occur.[13]

Interestingly, the electron diffraction experiments discussed above (Figure 5) indicate that in the present case the top and bottom facets of the product CdSe (and $CuInSe_2$) nanoplatelets consist of the polar (002) plane, while the side facets consist of the nonpolar (100) and (010) planes (Figure 6H). This implies that the reconstruction and structural transformation of the nanoplatelets result in growth of the polar (002) facets at the expenses of the nonpolar (100) and (010) side facets. Although this internal reconstruction process still involves transfer of material from high free-energy facets (the (002) top and bottom facets) to low free-energy facets (the nonpolar side facets), it is fundamentally different from typical internal ripening processes, since it results in growth of the high free energy facets rather than their elimination. This observation can be rationalized by considering that the polar top and bottom facets of the nanoplatelets are likely stabilized by dodecaneselenol, which can be expected to form dense ordered monolayers at surfaces, similarly to DDT and other linear chain alkylthiols.[23,28,51] Therefore, the increase in the relative area of the (002) facets most likely results in reduction of the overall surface free energy due to the stabilizing effect of surface ligands. The role of ligands in stabilizing facets is a well-known phenomenon.[19] For example, it has been shown that alkylamines stabilize the high energy (001) top and bottom facets of covellite CIS nanosheets,[52] oleic acid directs the 2D-growth of PbS by stabilizing the (100) facet,[53] and amines and DDT stabilize different djurleite $Cu_{2-x}S$ facets, thereby providing control over where CE reactions take place and consequently over the morphology of $Cu_{2-x}S/I-III-VI_2$ hetero-nanorods.[54] We thus conclude that the driving force for the internal reconstruction process that accompanies the structural transformation of the nanoplatelets from tetragonal umangite $Cu_{2-x}Se$ to hexagonal wurtzite CdSe and $CuInSe_2$ is likely the minimization of both the total surface free energy and the reconstruction strain during the structural reorganization process, in such a way that the total volume expansion work is kept to a minimum ($V_{Cu_2Se} = 1.7 \times 10^3$ nm^3, $V_{CdSe} = 2.1 \times 10^3$ nm^3, $V_{CuInSe_2} = 1.8 \times 10^3$ nm^3).

CONCLUSIONS

In this work, 1-dodecaneselenol (DDSe) was synthesized and used as Se-precursor for the synthesis of shape-controlled colloidal $Cu_{2-x}Se$ NCs with varying dimensions and shapes. During the $Cu_{2-x}Se$ NCs synthesis, Cu-DDSe complexes form that are stabilized by halides, similar to the $Cu_{2-x}S$ NCs synthesis using DDT as S-precursor. By adjusting the reaction parameters, the same control over size and shape can be achieved as for the analogue $Cu_{2-x}S$ system using DDT as S-precursor. However, the reaction temperatures required for the controlled synthesis of colloidal $Cu_{2-x}Se$ NCs from DDSe were found to be lower than those used for the S-analogue (viz., injection and growth at 130 and 170 °C instead of 160 and 220 °C, respectively). $Cu_{2-x}Se$ dot-shaped NCs ($d = 4.9 \pm 0.5$ nm), hexagonal nanoplatelets (4.4 ± 0.6 to 7.3 ± 0.6 nm thick with lateral dimensions from 21 ± 6 to 17 ± 2 nm), and ultrathin nanosheets (2.4 ± 0.4 nm thick with lateral dimensions ranging from ~50 to ~100 nm) were converted to wurtzite CdSe and $CuInS_2$ NCs through postsynthetic cation exchange reactions, yielding NCs with morphologies and dimensions that are not accessible via direct synthesis. Interestingly, although the overall shape of the template $Cu_{2-x}Se$ NCs was preserved in the product CdSe and $CuInS_2$ NCs, the cation exchange reactions were not fully topotactic, leading to a substantial reorganization of the anionic sublattice, which resulted in the change of the crystal structure from the tetragonal umangite to the hexagonal wurtzite and a NC reconstruction, through which the lateral dimensions of the nanoplatelets increased while their thicknesses decreased. This internal ripening process is likely driven by the minimization of both the total surface free energy (by creating more ligand coated top and bottom surfaces) and the reconstruction strain during the structural reorganization process (by keeping the total volume expansion work to a minimum). This work provides novel tools for the rational design of shape-controlled colloidal $Cu_{2-x}Se$ NCs, which, besides their promising optoelectronic properties, also constitute a new family of cation exchange templates for the synthesis of shape-controlled NCs of wurtzite CdSe, $CuInSe_2$, and other metal selenides that cannot be attained through direct synthesis approaches. Moreover, the insights provided here are likely applicable also to the direct synthesis of shape-controlled NCs of other metal selenides, since DDSe may be able to form lamellar complexes with several other metals.

ASSOCIATED CONTENT

Supporting Information

The Supporting Information is available free of charge on the ACS Publications website at DOI: 10.1021/acs.chemmater.8b01143.

^{13}C NMR spectrum of DDSe, ^{1}H NMR spectrum of DDSe-SeDD, TEM image of product material 1 min after DDSe injection in reaction mixture, size histograms of $Cu_{2-x}Se$ NCs, HR-TEM images of stacked $Cu_{2-x}Se$ NSs, TEM image and size histogram of control synthesis without halides, measured PL signals with two-sided Gaussian fit, PL decay curves of CdSe and $CuInSe_2$ quantum dots, TEM images and optical spectra of $Cu_{2-x}Se$ and CdSe nanoplatelets, size histograms of CdSe and $CuInSe_2$ NCs, HAADF-STEM elemental maps, HR-TEM images and ED ring patterns of $Cu_{2-x}Se$, CdSe, and $CuInSe_2$ NCs (PDF)

DOI: 10.1021/acs.chemmater.8b01143
Chem. Mater. 2018, 30, 3836−3846

AUTHOR INFORMATION

Corresponding Author

*E-mail c.demello-donega@uu.nl (C.d.M.D.).

ORCID

Ward van der Stam: 0000-0001-8155-5400

Celso de Mello Donega: 0000-0002-4403-3627

Present Addresses

W.v.d.S.: Optoelectronic Materials Section, Faculty of Applied Sciences, Delft University of Technology, van der Maasweg 9, 2629 HZ Delft, The Netherlands.

Q.A.A.: Nanochemistry Department, Istituto Italiano di Tecnologia, Via Morego 30, 16163 Genova, Italy.

Notes

The authors declare no competing financial interest.

ACKNOWLEDGMENTS

A.C.B. and C.d.M.D. acknowledge financial support from the division of Chemical Sciences (CW) of The Netherlands Organization for Scientific Research (NWO) under Grant ECHO.712.014.001. The authors are grateful to Vera Kaats (Chemistry Department, Utrecht University) for performing the NMR measurements.

REFERENCES

(1) van der Stam, W.; Berends, A. C.; de Mello Donegá, C. Prospects of Colloidal Copper Chalcogenide Nanocrystals. *ChemPhysChem* **2016**, *17*, 559−581.

(2) Coughlan, C.; Ibanez, M.; Dobrozhan, O.; Singh, A.; Cabot, A.; Ryan, K. M. Compound Copper Chalcogenide Nanocrystals. *Chem. Rev.* **2017**, *117*, 5865−6109.

(3) van der Stam, W.; Berends, A. C.; Rabouw, F. T.; Willhammar, T.; Ke, X.; Meeldijk, J. D.; Bals, S.; de Mello Donegá, C. Luminescent $CuInS_2$ Quantum Dots by Partial Cation Exchange in $Cu_{2-x}S$ Nanocrystals. *Chem. Mater.* **2015**, *27*, 621−628.

(4) Rivest, J. B.; Jain, P. K. Cation Exchange on the Nanoscale: An Emerging Technique for New Material Synthesis, Device Fabrication, and Chemical Sensing. *Chem. Soc. Rev.* **2013**, *42*, 89−96.

(5) Beberwyck, B. J.; Surendranath, Y.; Alivisatos, A. P. Cation Exchange: A Versatile Tool for Nanomaterials Synthesis. *J. Phys. Chem. C* **2013**, *117*, 19759−19770.

(6) Gupta, S.; Kershaw, S. V.; Rogach, A. L. 25th Anniversary Article: Ion Exchange in Colloidal Nanocrystals. *Adv. Mater.* **2013**, *25*, 6923−6944.

(7) de Trizio, L.; Manna, L. Forging Colloidal Nanostructures via Cation Exchange Reactions. *Chem. Rev.* **2016**, *116*, 10852−10887.

(8) van der Stam, W.; Bladt, E.; Rabouw, F. T.; Bals, S.; de Mello Donegá, C. Near-Infrared Emitting $CuInSe_2/CuInS_2$ Dot Core/Rod Shell Heteronanorods by Sequential Cation Exchange. *ACS Nano* **2015**, *9*, 11430−11438.

(9) Li, H.; Brescia, R.; Krahne, R.; Bertoni, G.; Alcocer, M. J. P.; D'Andrea, C.; Scotognella, F.; Tassone, F.; Zanella, M.; De Giorgi, M.; et al. Blue-UV-Emitting ZnSe (dot)/ZnS (rod) Core/Shell Nanocrystals Prepared from CdSe/CdS Nanocrystals by Sequential Cation Exchange. *ACS Nano* **2012**, *6*, 1637−1647.

(10) Groeneveld, E.; Witteman, L.; Lefferts, M.; Ke, X.; Bals, S.; van Tendeloo, G.; de Mello Donegá, C. Tailoring ZnSe-CdSe Colloidal Quantum Dots via Cation Exchange: From Core/Shell to Alloy Nanocrystals. *ACS Nano* **2013**, *7*, 7913−7930.

(11) Pietra, F.; Kirkwood, N.; de Trizio, L.; Hoekstra, A. W.; Kleibergen, L.; Renaud, N.; Koole, R.; Baesjou, P.; Manna, L.; Houtepen, A. J. Ga for Zn Cation Exchange Allows for Highly Luminescent and Photostable InZnP-based quantum dots. *Chem. Mater.* **2017**, *29*, 5192−5199.

(12) Berends, A. C.; de Mello Donegá, C. Ultrathin One- and Two-Dimensional Colloidal Semiconductor Nanocrystals: Pushing Quantum Confinement to the Limit. *J. Phys. Chem. Lett.* **2017**, *8*, 4077−4090.

(13) Donega, C. d. M. Synthesis and Properties of Colloidal Heteronanocrystals. *Chem. Soc. Rev.* **2011**, *40*, 1512−1546.

(14) Cunningham, P. D.; Souza, J. B.; Fedin, I.; She, C.; Lee, B.; Talapin, D. V. Assessment of Anisotropic Semiconductor Nanorod and Nanoplatelet Heterostructures with Polarized Emission for Liquid Crystal Display Technology. *ACS Nano* **2016**, *10*, 5769−5781.

(15) Cademartiri, L.; Ozin, G. A. Ultrathin Nanowires − A Materials Chemistry Perspective. *Adv. Mater.* **2009**, *21*, 1013−1020.

(16) Lee, D.; Kim, W. D.; Lee, S.; Bae, W. K.; Lee, S.; Lee, D. C. Direct Cd-to-Pb exchange of CdSe Nanorods into PbSe/CdSe Axial Heterojunction Nanorods. *Chem. Mater.* **2015**, *27*, 5295−5304.

(17) Groeneveld, E.; van Berkum, S.; van Schooneveld, M. M.; Gloter, A.; Meeldijk, J. D.; van den Heuvel, D. J.; Gerritsen, H. C.; de Mello Donegá, C. Highly Luminescent (Zn,Cd)Te-CdSe Colloidal Heteronanowires with Tunable Electron-Hole Overlap. *Nano Lett.* **2012**, *12*, 749−757.

(18) Li, H.; Brescia, R.; Povia, M.; Prato, M.; Bertoni, G.; Manna, L.; Moreels, I. Synthesis of Uniform Disk-Shaped Copper Telluride Nanocrystals and Cation Exchange to Cadmium Telluride Quantum Disks with Stable Red Emission. *J. Am. Chem. Soc.* **2013**, *135*, 12270−12278.

(19) Green, M. The Nature of Quantum Dot Capping Ligands. *J. Mater. Chem.* **2010**, *20*, 5797−5809.

(20) Bullen, C.; van Embden, J.; Jasieniak, J.; Cosgriff, J. E.; Mulder, R. J.; Rizzardo, E.; Gu, M.; Raston, C. L. High Activity Phosphine-Free Selenium Precursor Solution for Semiconductor Nanocrystal Growth. *Chem. Mater.* **2010**, *22*, 4135−4143.

(21) Jasieniak, J.; Bullen, C.; van Embden, J.; Mulvaney, P. Phosphine-Free Synthesis of CdSe Nanocrystals. *J. Phys. Chem. B* **2005**, *109*, 20665−20668.

(22) Hendricks, M. P.; Campos, M. P.; Cleveland, G. T.; Jen-La Plante, I.; Owen, J. S. A Tunable Library of Substituted Thiourea Precursors to Metal Sulfide nanocrystals. *Science* **2015**, *348*, 1226−1230.

(23) van der Stam, W.; Rabouw, F. T.; Geuchies, J. J.; Berends, A. C.; Hinterding, S. O. M.; Geitenbeek, R. G.; van der Lit, J.; Prévost, S.; Petukhov, A. V.; de Mello Donegá, C. *In Situ* Probing of Stack-Templated Growth of Ultrathin $Cu_{2-x}S$ Nanosheets. *Chem. Mater.* **2016**, *28*, 6381−6389.

(24) van der Stam, W.; Gradmann, S.; Altantzis, T.; Ke, X.; Baldus, M.; Bals, S.; de Mello Donegá, C. Shape Control of Colloidal $Cu_{2-x}S$ Polyhedral Nanocrystals by Tuning the Nucleation Rates. *Chem. Mater.* **2016**, *28*, 6705−6715.

(25) Bryks, W.; Smith, S. C.; Tao, A. R. Metallomesogen Templates for Shape Control of Metal Selenide Nanocrystals. *Chem. Mater.* **2017**, *29*, 3653−3662.

(26) Holligan, K.; Rogler, P.; Rehe, D.; Pamula, M.; Kornienko, A. Y.; Emge, T. J.; Krogh-Jespersen, K.; Brennan, J. G. Copper, Indium, Tin, and Lead Complexes with Fluorinated Selenolate Ligands: Precursors to MSex. *Inorg. Chem.* **2015**, *54*, 8896−8904.

(27) Froster, G.; Allen, C. F. H.; Cressman, H. W. J. Selenophenol. *Org. Synth.* **1944**, *24*, 89.

(28) van der Stam, W.; Akkerman, Q. A.; Ke, X.; van Huis, M. A.; Bals, S.; de Mello Donegá, C. Solution-Processable Ultrathin Size- and Shape-Controlled Colloidal $Cu_{2-x}S$ Nanosheets. *Chem. Mater.* **2015**, *27*, 283−291.

(29) Klinger, M.; Jäger, A. Crystallographic Tool Box (CrystTBox): Automated Tools for Transmission Electron Microscopists and Crystallographers. *J. Appl. Crystallogr.* **2015**, *48*, 2012−2018.

(30) Momma, K.; Izumi, F. VESTA 3 for Three-Dimensional Visualization of Crystal, Volumetric and Morphology data. *J. Appl. Crystallogr.* **2011**, *44*, 1272−1276.

(31) Merijanian, A.; Zingaro, R. A.; Sagan, L. S.; Irgolic, K. J. The ^{1}H(Se-H) NMR Chemical Shift in Selenols and the Fundamental Se-H Stretching Frequency. *Spectrochim. Acta Part A Mol. Spectrosc.* **1969**, *25*, 1160−1165.

DOI: 10.1021/acs.chemmater.8b01143
Chem. Mater. 2018, 30, 3836−3846

(32) Yagüe, J. L.; Agulló, N.; Fonder, G.; Delhalle, J.; Mekhalif, Z.; Borrós, S. Thiol versus Selenol SAMs as Nucleation Enhancers and Adhesion Promoters for Plasma Polymerized Pyrrole on Copper Substrates. *Plasma Processes Polym.* **2010**, *7*, 601−609.
(33) Espinet, P.; Lequerica, M. C. Synthesis, Structural Characterization and Mesogenic Behavior of Copper(i) N-Alkylthiolates. *Chem. - Eur. J.* **1999**, *5*, 1982−1986.
(34) *Shriver & Atkins − Inorganic Chemistry*, 5th ed.; Oxford Pub.: 2010.
(35) Bryks, W.; Lupi, E.; Ngo, C.; Tao, A. R. Digenite Nanosheets Synthesized by Thermolysis of Layered Copper-Alkanethiolate Frameworks. *J. Am. Chem. Soc.* **2016**, *138*, 13717−13725.
(36) de Mello Donegá, C.; Koole, R. Size Dependence of the Spontaneous Emission Rate and Absorption Cross Section of CdSe and CdTe Quantum Dots. *J. Phys. Chem. C* **2009**, *113*, 6511−6520.
(37) Efros, Al. L.; Rosen, M. The Electronic Structure Of Semiconductor Nanocrystals. *Annu. Rev. Mater. Sci.* **2000**, *30*, 475−521.
(38) Kolny-Olesiak, J.; Weller, H. Synthesis and Application of Colloidal $CuInS_2$ Semiconductor Nanocrystals. *ACS Appl. Mater. Interfaces* **2013**, *5*, 12221−12237.
(39) Berends, A. C.; Rabouw, F. T.; Spoor, F. C. M.; Bladt, E.; Grozema, F. C.; Houtepen, A. J.; Siebbeles, L. D. A.; de Mello Donegá, C. Radiative and Nonradiative Recombination in $CuInS_2$ Nanocrystals and $CuInS_2$-Based Core/Shell Nanocrystals. *J. Phys. Chem. Lett.* **2016**, *7*, 3503−3509.
(40) Yarema, O.; Bozyigit, D.; Rousseau, I.; Nowack, L.; Yarema, M.; Heiss, W.; Wood, V. Highly Luminescent, Size- and Shape-Tunable Copper Indium Selenide Based Colloidal Nanocrystals. *Chem. Mater.* **2013**, *25*, 3753−3757.
(41) Xia, C.; Meeldijk, J. D.; Gerritsen, H. C.; de Mello Donegá, C. Highly Luminescent Water-Dispersible NIR-Emitting Wurtzite $CuInS_2$/ZnS Core/Shell Colloidal Quantum Dots. *Chem. Mater.* **2017**, *29*, 4940−4951.
(42) Knowles, K.; Nelson, H. D.; Kilburn, T. B.; Gamelin, D. R. Singlet-Triplet Splittings in the Luminescent Excited States of Colloidal Cu^+:CdSe, Cu^+:InP and $CuInS_2$ Nanocrystals: Charge-Transfer Configurations and Self-Trapped Excitons. *J. Am. Chem. Soc.* **2015**, *137*, 13138−13147.
(43) Rice, W.; McDaniel, H.; Klimov, V. I.; Crooker, S. A. Magneto-Optical Properties of $CuInS_2$ Nanocrystals. *J. Phys. Chem. Lett.* **2014**, *5*, 4105−4109.
(44) Sharma, M.; Gungor, K.; Yeltik, A.; Olutas, M.; Guzelturk, B.; Kelestemur, Y.; Erdem, T.; Delikanli, S.; McBride, J. R.; Demir, H. V. Near-Unity Emitting Copper-Doped Colloidal Semiconductor Quantum Wells for Luminescent Solar Concentrators. *Adv. Mater.* **2017**, *29*, 1700821.
(45) Rice, K. P.; Saunders, A. E.; Stoykovich, M. P. Seed-Mediated Growth of Shape-Controlled Wurtzite CdSe Nanocrystals: Platelets, Cubes and Rods. *J. Am. Chem. Soc.* **2013**, *135*, 6669−6676.
(46) Olvera, A.; Sahoo, P.; Tarczynski, S.; Poudeu, P. F. P. Topochemical Solid-State Reactivity: Redox-Induced Direct Structural Transformation from $CuSe_2$ to $CuInSe_2$. *Chem. Mater.* **2015**, *27*, 7179−7186.
(47) Grodzinska, D.; Pietra, F.; van Huis, M. A.; Vanmaekelbergh, D.; de Mello Donegá, C. Thermally Induced Atomic Reconstruction of PbS/CdSe Core/Shell Quantum Dots into PbSe/CdSe Bi-Hemisphere Hetero-Nanocrystals. *J. Mater. Chem.* **2011**, *21*, 11556−11565.
(48) Min, Y.; Moon, G. D.; Park, J.; Park, M.; Jeong, U. Surfactant-Free $CuInSe_2$ Nanocrystals Transformed from In_2Se_3 Nanoparticles and their Application for a Flexible UV Photodetector. *Nanotechnology* **2011**, *22*, 465604.
(49) Xie, Y.; Bertoni, G.; Riedinger, A.; Sathya, A.; Prato, M.; Marras, S.; Tu, R.; Pellegrino, T.; Manna, L. Nanoscale Transformations in Covellite (CuS) Nanocrystals in the Presence of Divalent Metal Cations in a Mild Reducing Environment. *Chem. Mater.* **2015**, *27*, 7531−7537.
(50) Manna, L.; Wang, L. W.; Cingolani, R.; Alivisatos, A. P. First-Principles Modeling of Unpassivated and Surfactant-Passivated Bulk Facets of Wurtzite CdSe: A Model System for Studying the Anisotropic Growth of CdSe Nanocrystals. *J. Phys. Chem. B* **2005**, *109*, 6183−6192.
(51) Pileni, M. P. Nanocrystal Self-Assemblies: Fabrication and Collective Properties. *J. Phys. Chem. B* **2001**, *105*, 3358−3371.
(52) Berends, A. C.; Meeldijk, J. D.; van Huis, M. A.; de Mello Donegá, C. Formation of Colloidal Copper Indium Sulfide Nanosheets by Two- Dimensional Self-Organization. *Chem. Mater.* **2017**, *29*, 10551−10560.
(53) Schliehe, C.; Juarez, B. H.; Pelletier, M.; Jander, S.; Greshnykh, D.; Nagel, M.; Meyer, A.; Foerster, S.; Kornowski, A.; Klinke, C.; Weller, H. Ultrathin PbS Sheets by Two-Dimensional Oriented Attachment. *Science* **2010**, *329*, 550−553.
(54) Zhai, Y.; Flanagan, J. C.; Shim, M. Lattice Strain and Ligand Effects on the Formation of $Cu_{2-x}S$/I-III-VI_2 Nanorod Heterostructures through Partial Cation Exchange. *Chem. Mater.* **2017**, *29*, 6161−6167.

DOI: 10.1021/acs.chemmater.8b01143
Chem. Mater. 2018, 30, 3836−3846